

Field Reconstruction in Sensor Networks with Coverage Holes and Packet Losses

Alessandro Nordio^{*} and Carla-Fabiana Chiasserini[†]

^{*} IEIIT-CNR (Italian National Research Council), Torino, Italy

E-mail: alessandro.nordio@polito.it

[†] Dipartimento di Elettronica, Politecnico di Torino, Torino, Italy

E-mail: chiasserini@polito.it

Abstract

Environmental monitoring is often performed through a wireless sensor network, whose nodes are randomly deployed over the geographical region of interest. Sensors sample a physical phenomenon (the so-called field) and send their measurements to a *sink* node, which is in charge of reconstructing the field from such irregular samples. In this work, we focus on scenarios of practical interest where the sensor deployment is unfeasible in certain areas of the geographical region, e.g., due to terrain asperities, and the delivery of sensor measurements to the sink may fail due to fading or to transmission collisions among sensors simultaneously accessing the wireless medium. Under these conditions, we carry out an asymptotic analysis and evaluate the quality of the estimation of a d -dimensional field ($d \geq 1$) when the sink uses linear filtering as a reconstruction technique. Specifically, given the matrix representing the sampling system, \mathbf{V} , we derive both the moments and an expression of the limiting spectral distribution of $\mathbf{V}\mathbf{V}^H$, as the size of \mathbf{V} goes to infinity and its aspect ratio has a finite limit bounded away from zero. By using such asymptotic results, we approximate the mean square error on the estimated field through the η -transform of $\mathbf{V}\mathbf{V}^H$, and derive the sensor network performance under the conditions described above.

I. INTRODUCTION

Recently, a great deal of attention has been paid to wireless sensor networks whose nodes sample a physical phenomenon (hereinafter referred to as field), i.e., air temperature, light intensity, pollution levels or rain falls, and send their measurements to a central processing unit (or *sink* node). The sink is in charge of reconstructing the sensed field: if the field can be approximated as bandlimited in the time and space domain, then an estimate of the discrete spectrum can be obtained.

However, the sensors measurements typically represent an irregular sampling of the field of interest, thus the sink operates based on a set of field samples that are not regularly spaced in the time and

space domain. The reasons for such an irregular sampling are multifold. (i) The sensors may be irregularly deployed in the geographical region of interest, either due to the adopted deployment procedure (e.g., sensors thrown out of an airplane [1]), or due to the presence of terrain asperities and obstacles. (ii) The transmission of the measurements from the sensors to the central controller may fail due to bad channel propagation conditions (e.g., fading), or because collisions occur among the transmissions by sensors simultaneously attempting to access the channel. In this case, although the sample has been collected by the sensor, it will not be delivered to the central controller. (iii) The sensors may enter a low-power operational state (sleep mode), in order to save energy [2], [3]. While in sleep mode, the nodes neither perform sensing operations nor transmit/receive any measurement. (iv) The sensors may be loosely synchronized, hence sense the field at different time instants.

Clearly, sampling irregularities may result in a degradation of the reconstructed signal [4]. The work in [5] investigates this issue in the context of sensor networks. Other interesting studies can be found in [6] and [7], just to name a few, which address the perturbations of regular sampling in shift-invariant spaces [6] and the reconstruction of irregularly sampled images in presence of measure noise [7].

In this work, our objective is to evaluate the performance of the field reconstruction when the coordinates in the d -dimensional domain of the field samples, which reach the sink node, are randomly, independently distributed and the sensors measurements are noisy. We take as performance metric the mean square error (MSE) on the reconstructed field. As a reconstruction technique, we use linear filtering and we adopt the filter that minimizes the MSE (i.e., the LMMSE filter) [8]–[10]. The matrix representing the sampling system, in the following denoted by \mathbf{V} , results to be a d -fold Vandermonde matrix¹. By drawing on the results in [9], [11], we derive both the moments and an expression of the limiting spectral distribution (LSD) of $\mathbf{V}\mathbf{V}^H$, as the size of \mathbf{V} goes to infinity and its aspect ratio has a finite limit bounded away from zero. Then, by using such an asymptotic model, we approximate the MSE on the reconstructed field through the η -transform [12] of $\mathbf{V}\mathbf{V}^H$, and derive an expression for it. We apply our results to the study of network scenarios of practical interest, such as sensor sensor deployments with coverage holes, communication in presence of a fading channel, massively dense networks [13], [14], and networks using contention-based channel access techniques [15].

The rest of the paper is organized as follows. Section II reviews previous work, while Section III describes the system model under study. In Section IV, we first provide some useful definitions and introduce our performance metric, then we recall previous results on which we build our analysis. In Section V, we derive asymptotic results concerning the moments and the LSD of $\mathbf{V}\mathbf{V}^H$. Such results

¹An $n \times m$ matrix \mathbf{X} is Vandermonde if its (i, j) -th entry, $(\mathbf{X})_{ij}$ can be written as $(\mathbf{X})_{ij} = x_j^i$, $i = 0, \dots, n-1$, $j = 1, \dots, m$.

are applied to different practical scenarios in Section VI. Finally, Section VII concludes the paper.

II. RELATED WORK

In the context of sensor networks, several works [16]–[19] have studied the field reconstruction at the sink node in presence of spatial and temporal correlation among sensor measurements. In particular, in [19] the observed field is a discrete vector of target positions and sensor observations are dependent. By modeling the sensor network as a channel encoder and exploiting some concepts from coding theory, the network capacity, defined as the maximum value of the ratio of the target positions to the number of sensors, is studied as a function of the noise, the sensing function and the sensor connectivity level.

The paper by Dong and Tong [20] considers a dense sensor network where a MAC protocol is responsible to collect samples from network nodes. The work analyzes the impact of deterministic and random data collection strategies on the quality of field reconstruction. As a performance measure, the maximum of the reconstruction square error over the sensed field is employed, as opposed to our work where the mean square error is considered. Also, in [20] the field is a Gaussian random process and the sink always receives a sufficiently large number of samples so as to reconstruct the field with the required accuracy.

The problem of reconstructing a bandlimited field from a set of irregular samples at unknown locations, instead, has been addressed in [21]. There, the field is oversampled by irregularly spaced sensors; sensor positions are unknown but always equal to an integer multiple of the sampling interval. Different solution methods are proposed, and the conditions for which there exist multiple solutions or a unique solution are discussed. Differently from [21], we assume that the sink can either acquire or estimate the sensor locations and that the coordinates of the sampling points are randomly located over a finite d -dimensional domain.

As for previous results on Vandermonde matrices, in [11] Ryan and Debbah considered a Vandermonde matrix \mathbf{V} with $d = 1$ and complex exponential entries, whose phases are i.i.d. with continuous distribution. Under such hypothesis, they obtained the important results that, given the phases distribution, the moments of $\mathbf{V}\mathbf{V}^H$ can be derived once the moments for the case with uniformly distributed phases are known. Also, a method for computing the moments of sums and products of Vandermonde matrices, for the non-folded case (i.e., $d = 1$), has recently appeared in [22]; further insights on the extremal eigenvalues behavior, still for the case of non-folded Vandermonde matrices, can be found in [23]. Moreover, in [9] it has been shown that the LSD of $\mathbf{V}\mathbf{V}^H$ converges to the Marčenko-Pastur distribution [24] when \mathbf{V} is d -fold Vandermonde with uniformly distributed phases and $d \rightarrow \infty$.

Note that, with respect to previous studies on Vandermonde matrices with entries that are randomly

distributed on the complex unit circle, in this work we obtain results on the LSD of $\mathbf{V}\mathbf{V}^H$ where the entries of \mathbf{V} have phases drawn from a *generic continuous distribution*. By relying on the results in [9], [11], we show that such an LSD can be related to that of $\mathbf{V}\mathbf{V}^H$ when the phases of \mathbf{V} are *uniformly* distributed on the complex unit circle. We also provide some numerical results that show the validity of our analysis. To our knowledge, these results have not been previously derived. We then apply them to the study of several practical scenarios in the context of sensor networks, although our findings can be useful for the study of other aspects of communications as well [11].

III. NETWORK MODEL

We consider a network composed of m wireless sensors, which measure the value of a spatially-finite physical field defined over d dimensions, ($d \geq 1$). We denote by $\mathcal{H} = [-\frac{1}{2}, \frac{1}{2}]^d$ the hypercube over which the sampling points fall, and we assume that the sampling points are i.i.d. randomly distributed variables, whose value is known to the sink node. Note that this is a fair assumption, as one can think of sensor nodes randomly deployed over the geographical region that has to be monitored, or, even in the case where the network topology is intended to have a regular structure, the actual node deployment may turn out to be random due to obstacles or terrain asperities. In addition, now and then the sensors may enter a low-operational mode (hence become inactive) in order to save energy, and they may be loosely synchronized. All the above conditions yield a set of randomly distributed samples of the field under observation, in both the time and the space domain [5].

By truncating its Fourier series expansion, a physical field defined over d dimensions and with finite energy can be approximated in the region \mathcal{H} as [9]

$$n^{-d/2} \sum_{\ell} a_{\nu(\ell)} e^{j2\pi \ell^T \mathbf{x}} \quad (1)$$

where n is the approximate one-sided bandwidth (per dimension) of the field, $\ell = [\ell_1, \dots, \ell_d]^T$ is a vector of integers, with $\ell_k = 0, \dots, n-1$, $k = 1, \dots, d$. The coefficient $n^{-d/2}$ is a normalization factor and the function

$$\nu(\ell) = \sum_{j=1}^d n^{j-1} \ell_j,$$

maps uniquely the vector ℓ over $[0, n^d - 1]$. $a_{\nu(\ell)}$ denotes the $\nu(\ell)$ -th entry of the vector \mathbf{a} of size n^d , which represents the approximated field spectrum, while the real vectors \mathbf{x}_q , $q = 1, \dots, m$ represent the coordinates of the d -dimensional sampling points. In this work, we assume that \mathbf{x}_q , $q = 1, \dots, m$, are i.i.d. random vectors having a generic continuous distribution $f_x(\mathbf{z})$, $\mathbf{z} \in \mathcal{H}$. In the specific case where \mathbf{x}_q are i.i.d with i.i.d. entries x_{qj} , $j = 1, \dots, d$, uniformly distributed in $[-1/2, 1/2)$, we denote the distribution of \mathbf{x}_q by $f_u(\mathbf{z})$.

The coordinates of the d -dimensional sampling points, however, are known to the sink node, because (i) either sensors are located at pre-defined positions or their position can be estimated

through a localization technique [25], and (ii) the sampling time is either periodic or included in the information sent to the sink.

Now, let $\mathbf{s} = [s(\mathbf{x}_1), \dots, s(\mathbf{x}_m)]^T$ be the values of the samples at $[\mathbf{x}_1, \dots, \mathbf{x}_m]$, respectively. Following [8], [9], we can write the vector \mathbf{s} as a function of the field spectrum:

$$\mathbf{s} = \beta_{n,m}^{-1/2} \mathbf{V}^H \mathbf{a} \quad (2)$$

where \mathbf{V} is the $n^d \times m$ d -fold Vandermonde matrix with entries

$$(\mathbf{V}_{\nu(\ell),q}) = m^{-1/2} \exp(-2\pi i \ell^T \mathbf{x}_q) \quad (3)$$

randomly distributed on the complex circle of radius $m^{-1/2}$, and $\beta_{n,m}$ is the ratio of the rows to the columns of \mathbf{V} , i.e.,

$$\beta_{n,m} = \frac{n^d}{m}.$$

In general, the entries of \mathbf{a} can be correlated with covariance matrix $\mathbb{E}[\mathbf{a}\mathbf{a}^H]$. However, in the following, we restrict our attention to the class of fields characterized by $\mathbb{E}[\mathbf{a}\mathbf{a}^H] = \sigma_a^2 \mathbf{I}$.

In the case where the sensor measurements, $\mathbf{p} = [p_1, \dots, p_m]^T$, are noisy, then the relation between the sensor samples and the approximated field spectrum can be written as:

$$\mathbf{p} = \mathbf{s} + \mathbf{n} = \beta_{n,m}^{-1/2} \mathbf{V}^H \mathbf{a} + \mathbf{n} \quad (4)$$

where \mathbf{n} is a m -size, zero-mean random vector representing the noise. Here, we assume a white noise, i.e., with covariance matrix $\mathbb{E}[\mathbf{n}\mathbf{n}^H] = \sigma_n^2 \mathbf{I}_m$. Note that the additive white noise affecting the sensor measurements may be due to quantization, round-off errors or quality of the sensing device.

IV. PRELIMINARIES

In this section, we report some definitions and previous results that are useful for our study.

A. Useful definitions

Let us consider an $n \times n$ non-negative definite random matrix \mathbf{A} , whose eigenvalues are denoted by $\lambda_{\mathbf{A},1}, \dots, \lambda_{\mathbf{A},n}$.

Definition 4.1: The average empirical cumulative distribution of the eigenvalues of \mathbf{A} is defined as $F_{\lambda_{\mathbf{A}}}^{(n)}(z) = \frac{1}{n} \sum_{i=1}^n \mathbb{E}[1\{\lambda_{\mathbf{A},i} \leq z\}]$, where the superscript (n) indicates that we refer to a system with size n and $1\{\cdot\}$ is the indicator function. If $F_{\lambda_{\mathbf{A}}}^{(n)}(z)$ converges as $n \rightarrow \infty$, then $\lim_{n \rightarrow \infty} F_{\lambda_{\mathbf{A}}}^{(n)}(z) = F_{\lambda_{\mathbf{A}}}(z)$. The corresponding limiting probability density function, or limiting spectral distribution (LSD), is denoted by $f_{\lambda_{\mathbf{A}}}(\cdot)$.

Definition 4.2: The η -transform of \mathbf{A} is given by:

$$\eta_{\mathbf{A}}^{(n)}(\gamma) = \mathbb{E} \left[\text{tr} \left\{ (\gamma \mathbf{A} + \mathbf{I})^{-1} \right\} \right] = \mathbb{E} \left[\frac{1}{n} \sum_{i=1}^n \frac{1}{\gamma \lambda_{\mathbf{A},i} + 1} \right] \quad (5)$$

where $\text{tr}\{\cdot\}$ is the normalized matrix trace operator and γ is a non-negative real number. If $\eta_{\mathbf{A}}^{(n)}(\gamma)$ converges as $n \rightarrow \infty$, then the corresponding limit is $\eta_{\mathbf{A}}(\gamma) = \mathbb{E}[(\gamma\lambda_{\mathbf{A}} + 1)^{-1}]$ [12, p. 40], where $\lambda_{\mathbf{A}}$ is the generic asymptotic eigenvalue of \mathbf{A} , whose distribution is $f_{\lambda_{\mathbf{A}}}(z)$, and the average is computed with respect to $\lambda_{\mathbf{A}}$ [12].

Next, consider the matrix \mathbf{V} as defined in (3) and that the LMMSE filter is used for field reconstruction. Then, the estimate of the unknown vector \mathbf{a} in (4), given \mathbf{y} and \mathbf{V} , is obtained by computing $\hat{\mathbf{a}} = \mathbb{E}[\mathbf{a}\mathbf{p}^H]\mathbb{E}[\mathbf{p}\mathbf{p}^H]^{-1}\mathbf{p}$. Through easy computations and using the Sherman-Morrison-Woodbury identity, we can obtain the MSE as

$$\text{MSE}^{(n)} = \sigma_a^{-2} \mathbb{E} \left[\text{tr} \left\{ \left(\sigma_n^{-2} \beta_{n,m}^{-1} \mathbf{V}\mathbf{V}^H + \sigma_a^{-2} \mathbf{I} \right)^{-1} \right\} \right] = \eta_{\mathbf{V}\mathbf{V}^H}^{(n)} \left(\frac{\gamma}{\beta_{n,m}} \right) \quad (6)$$

where $\gamma = \sigma_a^2/\sigma_n^2$ denotes the signal-to-noise ratio on the sensor measurements, and we employed the definition of the η -transform given in (5).

Next, we approximate the MSE of the finite size system in (4) through an asymptotic model, which assumes the size of \mathbf{V} to grow to infinity while the ratio of its number of rows to its number of columns tends to a finite limit, β , greater than zero, i.e., we assume

$$\lim_{n,m \rightarrow \infty} \beta_{n,m} = \beta$$

Indeed, in our recent works [8]–[10] it was shown that this asymptotic model provides a tight approximation of the MSE of the finite size system, already for small values of n and m . Under these conditions, we therefore define the asymptotic expression of the MSE as [10]:

$$\text{MSE}_{\infty} = \lim_{n,m \rightarrow \infty} \text{MSE}^{(n)} = \eta_{\mathbf{V}\mathbf{V}^H}(\gamma/\beta) \quad (7)$$

if the limit exists.

B. Previous results

Vandermonde matrices have been studied in a number of recent works [8]–[11]. Specifically, [9] considered the case where the vectors \mathbf{x}_q are i.i.d., for $q = 1, \dots, m$, and their entries, x_{qj} are i.i.d. random variables with uniform distribution in $[-1/2, 1/2)$. The work there studied the eigenvalue distribution of $\mathbf{V}\mathbf{V}^H$ for both finite and infinite (i.e., $m, n \rightarrow \infty$) matrix size. Although an explicit expression of such LSD is still unknown, [9] provided an algorithm to compute its moments of any order in closed form.

Indeed, as $n, m \rightarrow \infty$ with $\beta_{n,m} = n^d/m$ having a finite limit $\beta > 0$, in [9] it was shown that the p -th moment of the generic asymptotic eigenvalue of $\mathbf{V}\mathbf{V}^H$, denoted by λ , is given by

$$M_{p,d,\beta,u} = \int z^p f_{\lambda,u}(d, \beta, z) dz = \sum_{k=1}^p \beta^{p-k} \sum_{\boldsymbol{\omega} \in \Omega_{p,k}} v(\boldsymbol{\omega})^d$$

where $f_{\lambda,u}(d, \beta, z)$ represents the distribution of λ . Moreover, $\Omega_{p,k}$ is the set of partitions of the set $\mathcal{P} = \{1, 2, \dots, p\}$ in k subsets, and $v(\omega) \in (0, 1]$, $\omega \in \Omega_{p,k}$ is a rational number that can be analytically computed from ω following the procedure described in [9]. The subscript u in $M_{p,d,\beta,u}$ and $f_{\lambda,u}(d, \beta, z)$ indicates that a uniform distribution of the entries of \mathbf{x}_q is considered in the matrix \mathbf{V} .

In [9] it was also shown that when $n, m, d \rightarrow \infty$, with $\beta_{n,m} = n^d/m$ having a finite limit $\beta > 0$, the eigenvalue distribution $f_{\lambda,u}(d, \beta, z)$ converges to the Marčenko-Pastur law [24]. A similar result [10] also applies when the vectors \mathbf{x}_q ($q = 1, \dots, m$) are independent but not i.i.d., with equally spaced averages.

More recently, Ryan and Debbah in [11] considered $d = 1$ and the case where the random variables x_{q1} , $q = 1, \dots, m$, are i.i.d. with continuous distribution $f_x(z)$, $0 \leq z < 1$. Under such hypothesis, it was shown that the asymptotic moments of $\mathbf{V}\mathbf{V}^H$ can be written as

$$M_{p,1,\beta,x} = \sum_{k=1}^p I_k \beta^{p-k} \sum_{\omega \in \Omega_{p,k}} v(\omega) \quad (8)$$

where the terms I_k depend on the phase distribution $f_x(z)$ and are given by

$$I_k = \int_0^1 f_x(z)^k dz$$

for $k \geq 1$. The subscript x in $M_{p,1,\beta,x}$ indicates that in the matrix \mathbf{V} the random variables x_{q1} have a generic continuous distribution $f_x(z)$. Note that for the uniform distribution we have $I_k = 1$, for all k . The important result in (8) states that, given β , if the moments of $\mathbf{V}\mathbf{V}^H$ are known for uniformly distributed phases, they can be readily obtained for any continuous phase distribution $f_x(z)$.

V. VANDERMONDE MATRICES WITH GENERIC PHASE DISTRIBUTION

In this work, we extend the above results by considering a sampling system defined over $d \geq 1$ dimensions with nonuniform sample distribution, where samples may be irregularly spaced in the time and spatial domains, as it occurs in wireless sensor networks. Being our goal the estimation of the quality of the reconstructed field, we aim at deriving the asymptotic MSE (i.e., $\eta_{\mathbf{V}\mathbf{V}^H}(\gamma/\beta)$).

We start by considering a generic continuous distribution, $f_x(\mathbf{z})$, $\mathbf{z} \in \mathcal{H}$ of the samples measured by the sensors over the d -dimensional domain. We state the theorem below, which gives the asymptotic expression of the generic moment of $\mathbf{V}\mathbf{V}^H$, for $d \geq 1$.

Theorem 5.1: Let \mathbf{V} a d -fold $n^d \times m$ Vandermonde matrix with entries given by (3) where the vectors \mathbf{x}_q , $q = 1, \dots, m$, are i.i.d. and have continuous distribution $f_x(\mathbf{z})$. Then, for $n, m \rightarrow \infty$, with $\beta_{n,m} = n^d/m$ having a finite limit $\beta > 0$, the p -th moment of $\mathbf{V}\mathbf{V}^H$ is given by

$$M_{p,d,\beta,x} = \sum_{k=1}^p \beta^{p-k} I_k \sum_{\omega \in \Omega_{p,k}} v(\omega)^d \quad (9)$$

where $I_k = \int_{\mathcal{H}} f_x(\mathbf{z})^k d\mathbf{z}$ and the terms $v(\omega)$ are defined as in [9].

The proof is given in Appendix A.

Using Theorem 5.1 and the definition of I_k , it is possible to show the theorem below, which provides the LSD of $\mathbf{V}\mathbf{V}^H$.

Theorem 5.2: Let

- \mathbf{V} be a d -fold $n^d \times m$ Vandermonde matrix with entries given by (3) where the vectors \mathbf{x}_q , $q = 1, \dots, m$, are i.i.d. and have continuous distribution $f_x(\mathbf{z})$, $\mathbf{z} \in \mathcal{H}$
- \mathcal{A} be the set where $f_x(\mathbf{z})$ is strictly positive, i.e., $\mathcal{A} = \{\mathbf{z} \in \mathcal{H} | f_x(\mathbf{z}) > 0\}$
- the cumulative density function

$$G_x(y) = \frac{1}{|\mathcal{A}|} |\{\mathbf{z} \in \mathcal{A} | f_x(\mathbf{z}) \leq y\}| \quad (10)$$

defined² for $y > 0$ and let $g_x(y)$ be its corresponding probability density function.

Then, the LSD of $\mathbf{V}\mathbf{V}^H$, for $n, m \rightarrow \infty$ with $\beta_{n,m} = n^d/m$ having a finite limit $\beta > 0$, is given by

$$f_{\lambda,x}(d, \beta, z) = (1 - |\mathcal{A}|) \delta(z) + |\mathcal{A}| \int_0^\infty \frac{g_x(y)}{y} f_{\lambda,u} \left(d, \frac{\beta}{y}, \frac{z}{y} \right) dy \quad (11)$$

Proof: The proof can be found in Appendix B. ■

From Theorem 5.2, the corollary below follows.

Corollary 5.1: Consider $f_x(\mathbf{z})$ such that $f_x(\mathbf{z}) > 0 \forall \mathbf{z} \in \mathcal{H}$. Then, let us denote by $f_{x'}(\mathbf{z})$ a scaled version of this function, so that

$$f_{x'}(\mathbf{z}) = \begin{cases} \frac{1}{|\mathcal{C}|} f_x \left(\frac{\mathbf{z}}{|\mathcal{C}|} \right) & \mathbf{z} \in \mathcal{C} \\ 0 & \mathbf{z} \in \mathcal{H} \setminus \mathcal{C} \end{cases} \quad (12)$$

where $\mathcal{C} \subset \mathcal{H}$. It can be shown that

$$f_{\lambda,x'}(d, \beta, z) = (1 - c) \delta(z) + c^2 f_{\lambda,x}(d, c\beta, cz) \quad (13)$$

where $c = |\mathcal{C}|$.

Proof: The proof can be found in Appendix C. ■

As an example of the result given in Corollary 5.1, consider that a unidimensional ($d = 1$) sensor network monitors the segment $\mathcal{H} = [-1/2, 1/2]$. Due to terrain irregularities and obstacles, nodes are deployed with uniform distribution only in the range $[-c/2, c/2]$ (with $c \in [0, 1]$). We therefore have $f_{x'}(z) = 1/c$ for $-c/2 \leq z \leq c/2$ and 0 elsewhere. Moreover, $f_{\lambda,x}(1, \beta, z) = f_{\lambda,u}(1, \beta, z)$. The expression of $f_{\lambda,x'}(1, \beta, z)$ is given by (13), by replacing $d = 1$ and the subscript x with the subscript u .

This result is well supported by simulations as shown in Figures 1(a) and 1(b). In the plots, we compare the asymptotic empirical spectral distribution (AESD) $f_{\lambda,x'}^{(n)}$ and $f_{\lambda,u}^{(n)}$ instead of the

² $|\mathcal{S}|$ denotes the measure of the set \mathcal{S}

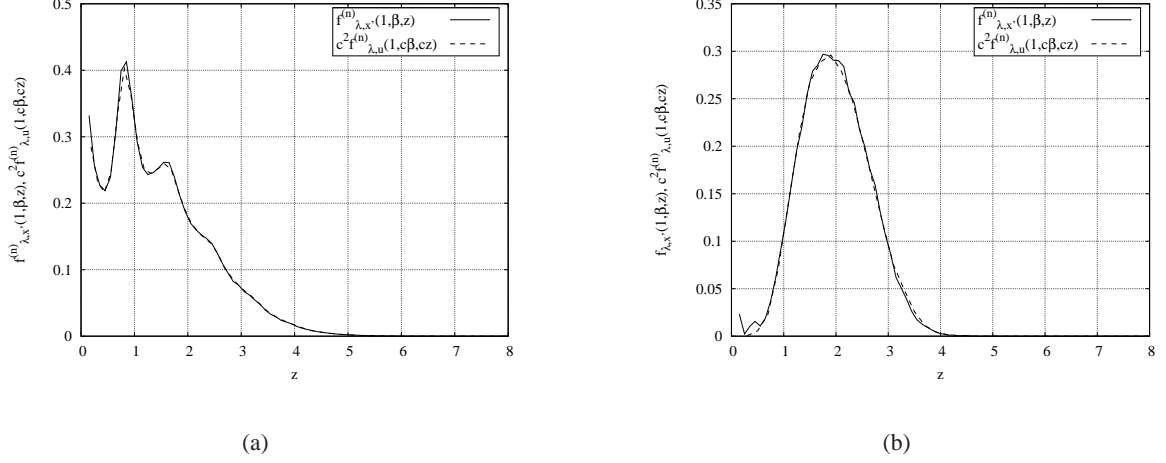


Fig. 1. Comparison between the curve representing $f_{\lambda,x'}^{(n)}(1, \beta_{n,m}, z)$ and the one representing the empirical function $c^2 f_{\lambda,u}^{(n)}(d, \beta_{n,m}c, zc)$. (a) $\beta_{n,m} = 0.8$, $c = 0.8$ and (b) $\beta_{n,m} = 0.2$, $c = 0.5$.

LSDs $f_{\lambda,x'}$ and $f_{\lambda,u}$ since an analytic expression of $f_{\lambda,u}$ is still unknown. However, in [8]–[10] it is shown that, already for small values of n , the AESD $f_{\lambda,u}^{(n)}$ appears to rapidly converge to a limiting distribution. Figure 1(a) refers to the case $\beta_{n,m} = 0.8$ and $c = 0.8$. The solid and dashed lines represent, respectively, the functions $f_{\lambda,x'}^{(n)}(1, \beta, z)$ and $c^2 f_{\lambda,u}^{(n)}(1, \beta_{n,m}c, zc)$, for $n = 100$. Note that the probability mass of $f_{\lambda,x'}^{(n)}(1, \beta_{n,m}, z)$ at $z = 0$ is not shown for simplicity. Similarly, Figure 1(b) shows the case $\beta_{n,m} = 0.2$ and $c = 0.5$. As evident from these plots, the match between the two functions is excellent for any parameter setting, thus supporting our findings.

Since we are interested in evaluating the MSE, taking into account the result in (7), we now apply the definition of the η -transform to (11). The corollary below immediately follows.

Corollary 5.2: The η -transform of $\mathbf{V}\mathbf{V}^H$ is given by

$$\eta_x(d, \beta, \gamma) = 1 - |\mathcal{A}| + |\mathcal{A}| \int_0^\infty g_x(y) \eta_u \left(d, \frac{\beta}{y}, \gamma y \right) dy \quad (14)$$

hence, the asymptotic MSE on the reconstructed field, defined in (7), is given by

$$\text{MSE}_\infty = \eta_x(d, \beta, \frac{\gamma}{\beta}) = 1 - |\mathcal{A}| + |\mathcal{A}| \int_0^\infty g_x(y) \eta_u \left(d, \frac{\beta}{y}, \frac{\gamma}{\beta} y \right) dy \quad (15)$$

Proof: The proof can be found in Appendix E. ■

In (14), in order to avoid a heavy notation we referred to $\eta_{\mathbf{V}\mathbf{V}^H}(d, \beta, \gamma)$ as $\eta_x(d, \beta, \gamma)$ when the phases of the entries of \mathbf{V} follow a generic random continuous distribution, while $\eta_u(d, \beta, \gamma)$ refers to the case where the phases are uniformly distributed.

Remark 5.1: Since $g_x(y) > 0$ and $\eta_u(d, \beta/y, \gamma y/\beta) > 0$, the integral in the right hand side of (14) is positive, then $\eta_x(d, \beta, \gamma/\beta) > 1 - |\mathcal{A}|$. It follows that the MSE is lower-bounded by the measure of the total area where the probability of finding a sensor is zero. This clearly suggests that, in order

to obtain a good quality of the field reconstructed at the sink node, this area must be a small fraction of the region under observation.

Next, we observe that, in the case of massively dense networks where the number of sampling sensors is much larger than the number of harmonics considered in the approximated field, i.e., $\beta \ll 1$, an interesting result holds:

Corollary 5.3: Let \mathcal{A} be the set where $f_x(\mathbf{z})$ is strictly positive; then

$$\lim_{\beta \rightarrow 0} f_{\lambda,x}(d, \beta, z) = (1 - |\mathcal{A}|) \delta(z) + |\mathcal{A}| g_x(z) \quad (16)$$

Proof: The proof can be found in Appendix D. ■

Thus, as evident from Corollary 5.3, for the limit of $\beta \rightarrow 0$, the LSD of $\mathbf{V}\mathbf{V}^H$ is the density of the density of the phase distribution $f_x(\mathbf{z})$.

Furthermore, for massively dense networks, we have:

Corollary 5.4: Let \mathcal{A} be the set where $f_x(\mathbf{z})$ is strictly positive; then

$$\lim_{\beta \rightarrow 0} \eta_x(d, \beta, \gamma/\beta) = 1 - |\mathcal{A}| \quad (17)$$

Proof: The proof can be found in Appendix F. ■

Remark 5.2: The result in (17) shows that even for massively dense networks $1 - |\mathcal{A}|$ is the minimum achievable MSE_∞ , when an area \mathcal{A} cannot be covered by sensors.

VI. FIELD RECONSTRUCTION IN PRESENCE OF LOSSES

Here, we provide examples of how our results can be used in wireless sensor networks to investigate the impact of a random distribution of the coordinates of the sampling points on the quality of the reconstructed field. In particular, we first consider a wireless channel affected by fading, and then the effects of contention-based channel access.

A. Sensor network performance with fading communication channel

We consider a wireless sensor network whose nodes are uniformly distributed over a geographical region. Without loss of generality, we assume a square region of unitary side ($d = 2$, $\mathcal{H} = [-1/2, +1/2]^2$), where the sink is located at the center and has coordinates $(z_1, z_2) = (0, 0)$. Through direct transmissions, the sensors periodically send messages to the sink, including their measurements. At every sample period, a sensor message is correctly received at the sink if its signal-to-noise ratio (SNR) exceeds a threshold τ . The communication channel is assumed to be affected by slow fading and to be stationary over the message duration.

Let d be the distance between a generic sensor and the sink. Then, the signal to noise ratio at the receiver is given by

$$\text{SNR}(d) = s|h|^2 d^{-2}$$

where $h \sim \mathcal{N}_{\mathbb{C}}(0, 1)$ is a circularly symmetric Gaussian complex random variable representing the channel gain, and s is the signal to noise ratio in the absence of fading and when the sensor-sink distance is $d = 1$.

The probability that a message is correctly received at the sink is given by

$$\begin{aligned} \mathbb{P}(\text{SNR}(d) > \tau) &= \mathbb{P}\left(|h|^2 > \tau \frac{d^2}{s}\right) \\ &= 1 - F_{|h|^2}\left(\tau \frac{d^2}{s}\right) \\ &= \exp(-ad^2) \end{aligned} \quad (18)$$

with $a = \tau/s$ and $F_{|h|^2}(z) = 1 - e^{-z}$ being the cumulative density function of $|h|^2$.

The probability density $f_x(z_1, z_2)$ corresponding to sensors at distance $d = \sqrt{z_1^2 + z_2^2}$, $-1/2 \leq z_1, z_2 \leq 1/2$ from the sink and successfully sending a message is then given by

$$f_x(z_1, z_2) = \frac{f_u(z_1, z_2) \mathbb{P}\left(\text{SNR}\left(\sqrt{z_1^2 + z_2^2}\right) > \tau\right)}{\iint_{\mathcal{H}} f_u(z_1, z_2) \mathbb{P}\left(\text{SNR}\left(\sqrt{z_1^2 + z_2^2}\right) > \tau\right) dz_1 dz_2}$$

where $f_u(z_1, z_2) = 1 \forall z_1, z_2$, is the density representing the sensor deployment (recall that nodes are assumed to be uniformly distributed in the region hence their density is constant and equal to 1).

Using (18), we obtain:

$$\begin{aligned} f_x(z_1, z_2) &= \frac{\exp(-a(z_1^2 + z_2^2))}{\iint_{\mathcal{H}} \exp(-a(z_1^2 + z_2^2)) dz_1 dz_2} \\ &= b \exp(-a(z_1^2 + z_2^2)) \end{aligned} \quad (19)$$

where

$$b^{-1} = \iint_{\mathcal{H}} \exp(-a(z_1^2 + z_2^2)) dz_1 dz_2 = \frac{\pi}{a} \text{erf}^2\left(\sqrt{\frac{a}{4}}\right)$$

In order to compute (14), we need the function $g_x(y)$, i.e., the density of $f_x(z_1, z_2)$. Note that $f_x(z_1, z_2)$ is circularly symmetric with respect to $(z_1, z_2) = (0, 0)$. Let y be the value of density of the sampling points at distance $d_y = \sqrt{z_1^2 + z_2^2}$ from the sink. Then, from (19) we obtain $d_y = \sqrt{\frac{1}{a} \log \frac{b}{y}}$, thus the network area where the density is lower than y is given by

$$G_x(y) = 1 - \pi d_y^2$$

for $0 \leq d_y \leq 1/2$, i.e., $be^{-a/4} \leq y < b$. For $1/2 < d_y < \sqrt{2}/2$, it is possible to show that

$$G_x(y) = 1 - \sqrt{4d_y^2 - 1} - d_y^2 \left(\pi - 4 \cos^{-1} \frac{1}{2d_y} \right)$$

In conclusion,

$$G_x(y) = \begin{cases} 1 & y/b \geq 1 \\ 1 - \pi d_y^2 & e^{-a/4} \leq y/b < 1 \\ 1 - \sqrt{4d_y^2 - 1} - d_y^2 \left(\pi - 4 \cos^{-1} \frac{1}{2d_y} \right) & e^{-a/2} \leq y/b < e^{-a/4} \\ 0 & y/b < e^{-a/2} \end{cases} \quad (20)$$

and

$$g_x(y) = \begin{cases} 0 & y/b \geq 1 \\ \frac{\pi}{ay} & e^{-a/4} \leq y/b < 1 \\ \frac{1}{ay} \left(\pi - 4 \cos^{-1} \frac{1}{2d_y} \right) & e^{-a/2} \leq y/b < e^{-a/4} \\ 0 & y/b < e^{-a/2} \end{cases} \quad (21)$$

Since $|\mathcal{A}| = 1$, then the asymptotic MSE can be obtained by computing

$$\text{MSE}_\infty = \eta_x(2, \beta, \gamma/\beta) = \int_{e^{-a/2}}^b g_x(y) \eta_u \left(2, \frac{\beta}{y}, \frac{\gamma y}{\beta} \right) dy \quad (22)$$

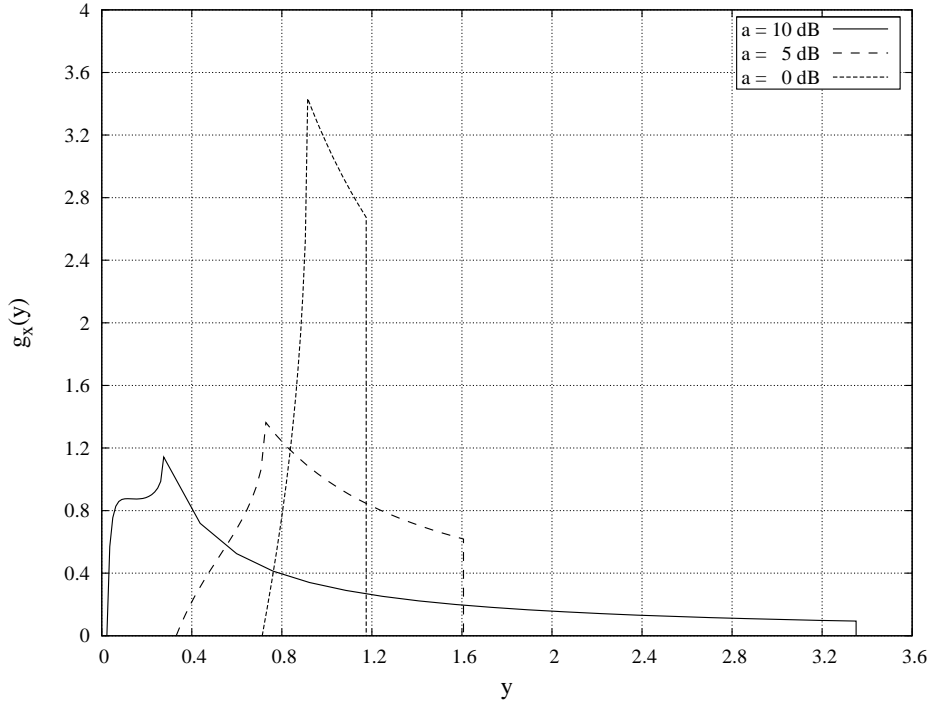


Fig. 2. Transmissions in presence of fading: density $g_x(y)$ for $a = 0, 5, 10$ dB, i.e., for different values of the SNR threshold τ .

Figure 2 shows the density $g_x(y)$ for $a = 0, 5, 10$ dB. Note that $a = \tau/s$, thus for a fixed s (i.e., the signal to noise ratio at distance D in the absence of fading) the parameter a is proportional to the SNR threshold τ . In particular, as τ decreases, the probability that a message successfully reaches the destination increases and, thus, the spatial distribution of correctly received samples, $f_x(z_1, z_2)$, tends to the uniform distribution $f_u(z_1, z_2)$. As a consequence, the density of $f_x(z_1, z_2)$, i.e., $g_x(y)$, for $a = 0$ and 5 dB is concentrated close to $y = 1$. However, for high values of τ , messages originated from sensor nodes located far from the sink are successfully received with low probability. Thus, $g_x(y)$ shows a significant probability mass around $y = 0$.

Figure 3 shows the effect of the fading channel on the MSE of the reconstructed field (dashed lines), and compares the obtained results with the MSE obtained in absence of fading (solid lines).

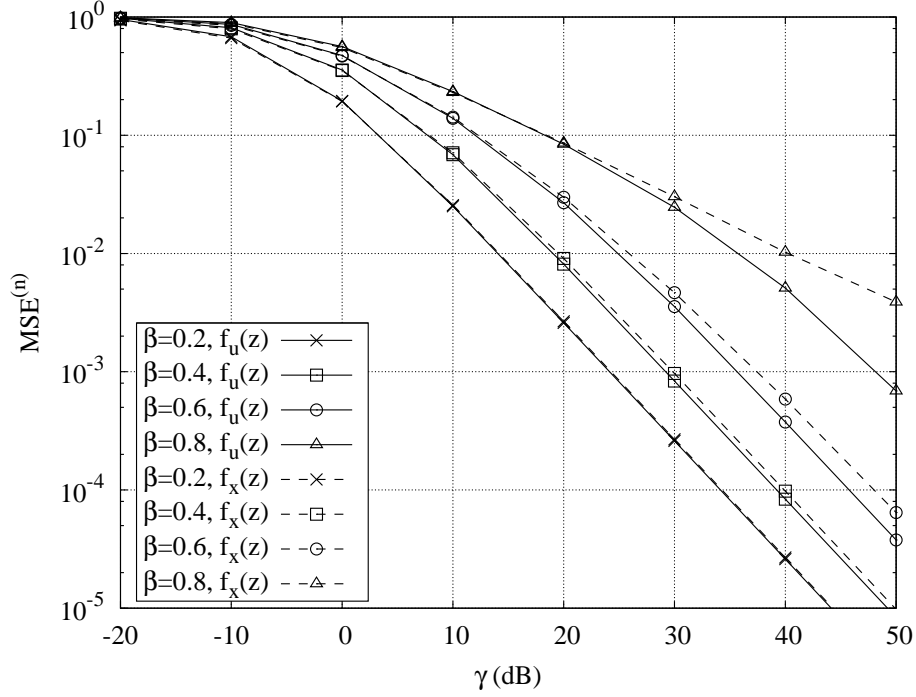


Fig. 3. MSE of the reconstructed field in absence ($f_u(\mathbf{z})$) and in presence ($f_x(\mathbf{z})$) of fading, as the signal to noise ratio on the sensor measurements varies.

The plot considers different values of β , namely, $\beta = 0.2, 0.4, 0.6, 0.8$, and $a = 5$ dB. The MSE is plotted versus the signal to noise ratio on the sensor measurements, γ . The curves have been obtained by numerically computing (22), where $g_x(y)$ is given by (21) and $\eta_u(2, \beta, \gamma/\beta)$ is replaced by $\eta_u^{(n)}(2, \beta_{n,m}, \gamma/\beta_{n,m})$, with $n = 10$. Recall that the analytic expression of the LSD $f_{\lambda,u}(d, \beta, z)$ is unknown, hence in the numerical results we considered the AESD $f_{\lambda,u}^{(n)}(d, \beta_{n,m}, z)$ instead. We observe that for low values β , in spite of the presence of fading, the sink node still receives a large number of samples from the sensors, hence the degradation of the MSE shown in Figure 3 is negligible. On the contrary, for $\beta > 0.4$ (i.e., for a larger value of the ratio of the number of harmonics composing the approximated field to the number of sensors), the reconstruction performance degrades significantly and this is particularly evident in presence of high values of γ .

In the case of massively dense networks, the LSD of $\mathbf{V}\mathbf{V}^H$ is given by (16) and from (17) we know that the MSE tends to 0 as $\beta \rightarrow \infty$. This result is confirmed by the plot in Figure 4, which shows the AESD $f_{\lambda,x}^{(n)}(2, \beta_{n,m}, z)$, for $|\mathcal{A}| = 1$, $a = 5$ dB, and $n = 10$. The behavior of such a function is compared with the density $g_x(z)$ as β varies. We note that, as β decreases, the matching between $f_{\lambda,x}^{(n)}(2, \beta_{n,m}, z)$ and $g_x(z)$ improves, and the latter represents an excellent approximation already for $\beta = 0.01$, as predicted by the result in (5.3).

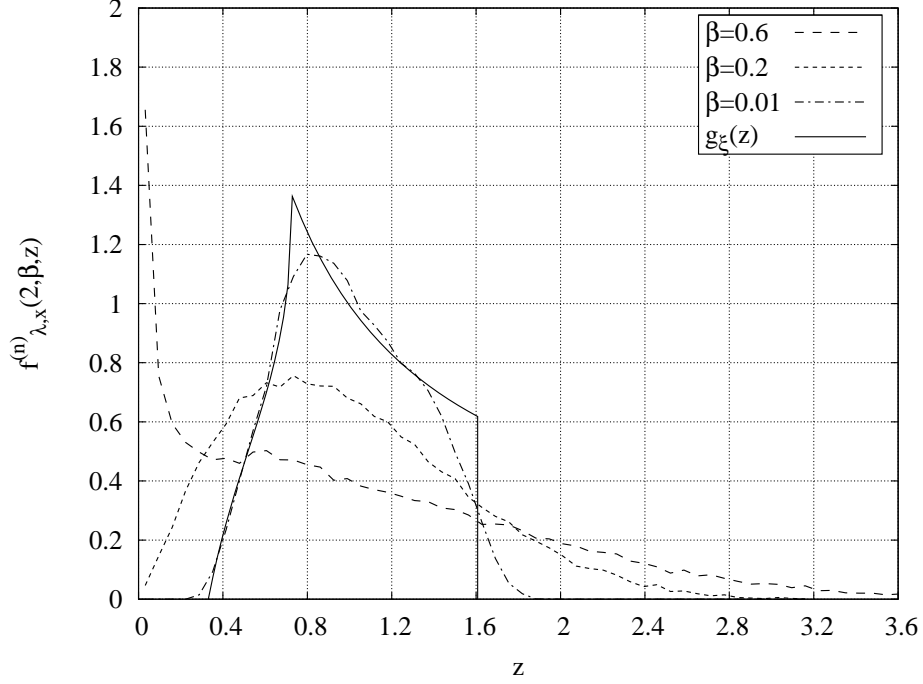


Fig. 4. Massively dense networks: empirical function $f_{\lambda,x}^{(n)}(2, \beta, z)$ in presence of fading, with $a = 5$ dB and $|\mathcal{A}| = 1$. The curves obtained for different values of β are compared with the density $g_x(z)$.

B. Measurements gathering through contention-based channel access

In environmental monitoring applications, it is often desirable to vary the resolution level with which the field measurements are taken over the region under observation, depending on the field variations and the interest level of the different locations [2], [3]. It follows that the number of samples generated by the sensors network (i.e., the offered traffic load) varies in the spatial domain.

To represent such a scenario, we consider a wireless sensor network whose nodes are uniformly deployed over a square region. We also identify L areas, A_i $i = 1, \dots, L$, each corresponding to a different value of the offered traffic load. As often assumed in the literature (see e.g., [26], [27]) and widely applied in the practice, the network is divided into clusters and a hierarchy of clusters is created. More specifically, at the first hierarchical layer, layer 1, the sensors are grouped into clusters, each of which is controlled by a cluster-head. The cluster-head is in charge of handling all traffic packets it receives from the nodes. At a given layer $h > 1$ of the hierarchy, the cluster-heads are grouped into clusters on their turn and forward the traffic to their parent cluster-head. At the highest layer, layer H , we have only one cluster whose cluster-head coincides with the sink node. Without loss of generality, we assume that the cluster at the H -th layer is composed of L cluster-heads, each handling the traffic generated within one of the L areas defined above.

As for the medium access control (MAC) layer, we consider that the nodes implement the IEEE

802.15.4 standard specifications for wireless sensor networks [15]. In particular, all nodes within a cluster are in radio visibility of each other and use the slotted carrier-sense multiple-access/collision avoidance (CSMA/CA) technique [15]. This is a contention-based scheme and transmissions may fail if two or more sensors access the channel at the same time. Inter-cluster interference is instead avoided by assigning different frequency channels to neighboring clusters. We consider that packets, whose transmission fails, are discarded.

In order to derive the probability that a packet transmission fails within a cluster due to collision, we use the Markov chain model presented in [28]. We denote by $m_{i,h}$ the average number of sensors belonging to the generic cluster at the h -th layer of the hierarchical architecture, in area A_i ($i = 1, \dots, L$ and $h = 1, \dots, H$). Similarly, we define $\lambda_{i,h}$ as the average traffic load per node, again within the generic cluster at the h -th layer, in area A_i . Then, we set the size of the packet payload to 32 bytes, and the value of the other parameters as in [28]. Under this setting, we compute the value of the collision probability within the generic cluster at layer h , in area A_i , as a function of $m_{i,h}$ and $\lambda_{i,h}$, i.e., $P_c(i, h)$ [28]. Furthermore, we observe that at the generic layer h , with $1 < h \leq H$, a node, which acts as cluster-head at layer $h - 1$ in area A_i , will have a traffic load equal to $\lambda_{i,h} = m_{i,h-1} \lambda_{i,h-1} [1 - P_c(i, h - 1)]$.

It follows that the probability that a packet is successfully delivered to the corresponding h -layer cluster-head within area A_i ($i = 1, \dots, L$) can be obtained as $P_s(i, h) = 1 - P_c(i, h)$. Then, the probability that a measurement generated by a sensor located in A_i ($i = 1, \dots, L$) is successfully delivered to the sink is given by:

$$P_s(i) = 1 - \prod_{h=1}^H P_c(i, h).$$

Next, denoting by $|A_i|$ the measure of A_i , we define

$$p_s(i) = \frac{P_s(i)}{\sum_{i=1}^L |A_i| P_s(i)}$$

as the normalized probability that a message is successfully delivered to the sink. Then, the spatial density of the sensors successfully sending their message is as follows:

$$f_x(z_1, z_2) = p_s(i) \quad \forall (z_1, z_2) \in A_i, \quad i = 1, \dots, L.$$

The density of $f_x(z_1, z_2)$ is therefore given by

$$g_x(y) = \sum_{i=1}^L |A_i| \delta(y - p_s(i)).$$

and the asymptotic MSE is given by

$$\text{MSE}_\infty = \eta_x(2, \beta, \frac{\gamma}{\beta}) = \sum_{i=1}^L |A_i| \eta_u\left(2, \frac{\beta}{p_s(i)}, \frac{\gamma}{\beta} p_s(i)\right)$$

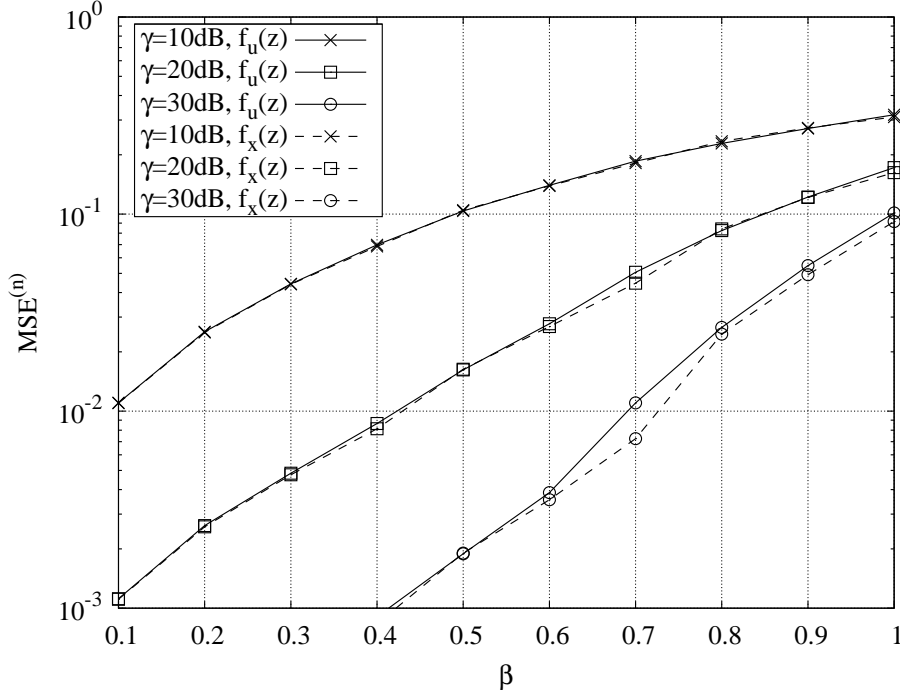


Fig. 5. Comparison between the case where transmission collisions are taken into account ($f_x(\mathbf{z})$) and the case where all measurements successfully reach the sink ($f_u(\mathbf{z})$). The MSE is shown as a function of β and for different values of signal-to-noise ratio ($H = 3$, $|A_i| = 1/4, \forall i$, $\lambda_{1,1} = 10^{-3}$, $\lambda_{2,1} = 2 \cdot 10^{-4}$, $\lambda_{3,1} = 2 \cdot 10^{-4}$, $\lambda_{4,1} = 2 \cdot 10^{-5}$).

Figures 5 and 6 show the impact of collisions due to the contention-based channel access, on the quality of the reconstructed field. In particular, they compare the MSE of the reconstructed field when collisions are taken into account ($f_x(\mathbf{z})$) with the one obtained in the idealistic case where all messages (measurements) sent by the sensors successfully reach the sink ($f_u(\mathbf{z})$). The results refer to a square region of unitary side, where there are four areas of equal size ($|A_i| = 1/4, i = 1, \dots, 4$) but corresponding to different resolution levels in the measurements collection (i.e., they are characterized by different traffic loads); the number of hierarchical levels is set to $H = 3$. We set $\lambda_{1,1} = 10^{-3}$, $\lambda_{2,1} = 2 \cdot 10^{-4}$, $\lambda_{3,1} = 2 \cdot 10^{-4}$, $\lambda_{4,1} = 2 \cdot 10^{-5}$ in Figure 5, and a higher traffic load in Figure 6, i.e., $\lambda_{1,1} = 5 \cdot 10^{-3}$, $\lambda_{2,1} = 10^{-3}$, $\lambda_{3,1} = 10^{-3}$, $\lambda_{4,1} = 10^{-4}$.

Looking at the plots, we observe that both β and γ have a significant impact of the obtained MSE, with the MSE increasing as β grows and smaller values of γ are considered. Most interestingly, by comparing the two figures, we can see that as the traffic load, hence the collision probability, increases, the performance derived taking into account the contention-based channel access significantly differs from the idealistic one. Furthermore, the latter effect is particularly evident as γ increases, since the higher the signal-to-noise ratio, the more valuable the samples sent by the sensors toward the sink.

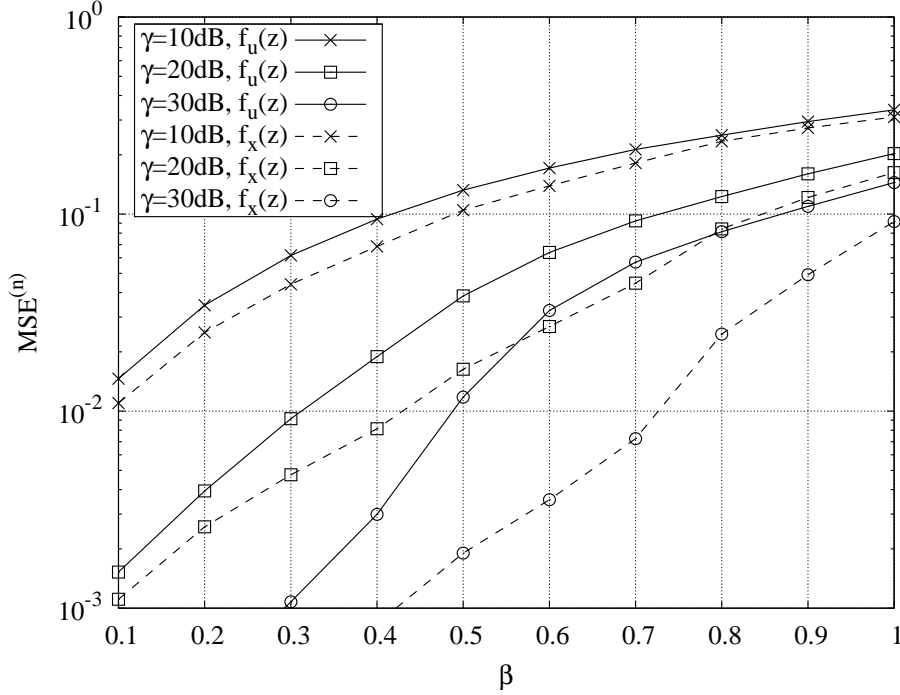


Fig. 6. Comparison between the case where transmission collisions are taken into account ($f_x(\mathbf{z})$) and the case where all measurement transmissions are successful ($f_u(\mathbf{z})$). The MSE is shown as β varies and for different values of signal-to-noise ratio ($H = 3$, $|A_i| = 1/4, \forall i$, $\lambda_{1,1} = 5 \cdot 10^{-3}$, $\lambda_{2,1} = 10^{-3}$, $\lambda_{3,1} = 10^{-3}$, $\lambda_{4,1} = 10^{-4}$).

VII. CONCLUSION

We studied the performance of a wireless network whose nodes sense a multi-dimensional field and transfer their measurements to a sink node. As often happens in practical cases, we assumed the sensors to be randomly deployed over (the whole or only a portion of) the region of interest, and that their measurements may be lost due to fading or transmission collisions over the wireless channel. We modeled the sampling system through a multi-folded Vandermonde matrix \mathbf{V} and, by using asymptotic analysis, we approximated the MSE of the field, which the sink node reconstructs from the received sensor measurements with the η -transform of $\mathbf{V}\mathbf{V}^H$.

Our results clearly indicate that the percentage of region where sensors cannot be deployed must be extremely small if an accurate field estimation has to be obtained. Also, the effect of losses due to fading or transmission collisions can be greatly mitigated provided that a suitable value for the ratio between the number of harmonics approximating the field bandwidth and the number of sensors is selected.

APPENDIX A

PROOF OF THEOREM 5.1

The p -th moment of the asymptotic eigenvalue distribution of $\mathbf{V}\mathbf{V}^H$ can be expressed as [9]

$$M_{p,d,\beta,x} = \lim_{n,m \rightarrow \infty} \mathbb{E} \left[\text{tr} \left\{ \left(\mathbf{V}\mathbf{V}^H \right)^p \right\} \right]$$

where $\text{tr}\{\cdot\}$ is the normalized matrix trace operator. The matrix power can be expanded as a multiple sum over the entries of \mathbf{V} :

$$M_{p,d,\beta,x} = \lim_{n,m \rightarrow \infty} \frac{1}{m^p n^d} \sum_{\ell_1, \dots, \ell_p} \sum_{q_1, \dots, q_p} \mathbb{E} \left[e^{j2\pi \ell_1^T (\mathbf{x}_{q_p} - \mathbf{x}_{q_1})} \dots e^{-j2\pi \ell_p^T (\mathbf{x}_{q_{p-1}} - \mathbf{x}_{q_p})} \right]$$

where q_1, \dots, q_p , $q_i = 1, \dots, m$ are integer indices and ℓ_1, \dots, ℓ_p , $\ell_i = [\ell_{i,1}, \dots, \ell_{i,d}]^T$, $\ell_{i,j} = 0, \dots, n-1$ are the indices identifying the rows of \mathbf{V} . Since,

$$\sum_{\ell_i} e^{j2\pi \ell_i^T \mathbf{x}} = \sum_{\ell_{i,1}, \dots, \ell_{i,d}=0}^{n-1} e^{j2\pi (\ell_{i,1}x_1 + \dots + \ell_{i,d}x_d)} = \prod_{j=1}^d \frac{1 - e^{j2\pi n x_j}}{1 - e^{j2\pi x_j}}$$

for $i = 1, \dots, p$ and the elements of \mathbf{x} are i.i.d., we have that

$$M_{p,d,\beta,x} = \lim_{n,m \rightarrow \infty} \frac{1}{m^p n^d} \sum_{q_1, \dots, q_p} \mathbb{E} \left[\prod_{i=1}^p \prod_{j=1}^d \frac{1 - e^{j2\pi n (x_{q_i,j} - x_{q_{i+1},j})}}{1 - e^{j2\pi (x_{q_i,j} - x_{q_{i+1},j})}} \right]$$

where the index i is to be considered modulo p , i.e., $p+1 \equiv 1$. As for the sum over the indices q_1, \dots, q_p we note that any choice of $\mathbf{q} = [q_1, \dots, q_p]^T$ induces a partition ω of the set, $\mathcal{P} = \{1, \dots, p\}$ in k subsets $\mathcal{P}_1, \dots, \mathcal{P}_k$, $1 \leq k \leq p$, under the equality relation [9]. In the following, we denote by $\Omega_{p,k}$ the set of partitions of \mathcal{P} in k subsets, $1 \leq k \leq p$. Since there are m^k possible vectors \mathbf{q} inducing a given partition $\omega \in \Omega_{p,k}$, we can write the p -th moment as

$$\begin{aligned} M_{p,d,\beta,x} &= \lim_{n,m \rightarrow \infty} \sum_{k=1}^p \sum_{\omega \in \Omega_{p,k}} \frac{\beta_{n,m}^{p-k}}{n^{d(p-k+1)}} \mathbb{E} \left[\prod_{i=1}^p \prod_{j=1}^d \frac{1 - e^{j2\pi n (x_{\omega_i,j} - x_{\omega_{i+1},j})}}{1 - e^{j2\pi (x_{\omega_i,j} - x_{\omega_{i+1},j})}} \right] \\ &= \lim_{n,m \rightarrow \infty} \sum_{k=1}^p \beta_{n,m}^{p-k} \sum_{\omega \in \Omega_{p,k}} \frac{\mathbb{E} [\Phi_{\omega}(\mathbf{x}_1, \dots, \mathbf{x}_k)]}{n^{d(p-k+1)}} \end{aligned} \quad (23)$$

where $\Phi_{\omega}(\mathbf{x}_1, \dots, \mathbf{x}_k) = \prod_{j=1}^d F_{\omega}(x_{1j}, \dots, x_{kj})$, $F_{\omega}(x_{1j}, \dots, x_{kj}) = \prod_{i=1}^p \frac{1 - e^{j2\pi n (x_{\omega_i,j} - x_{\omega_{i+1},j})}}{1 - e^{j2\pi (x_{\omega_i,j} - x_{\omega_{i+1},j})}}$, and $\omega_i \in \{1, \dots, k\}$ is the index of the subset of \mathcal{P} containing i . Recall that $p+1 \equiv 1$ and that $\beta_{n,m} = n^d/m$. Moreover, since the vectors \mathbf{x} are i.i.d., we removed the dependence on the subscript q .

Following the same steps as in [11, Appendix H], we compute the limit

$$\begin{aligned} \lim_{n \rightarrow \infty} \frac{\mathbb{E} [\Phi_{\omega}(\mathbf{x}_1, \dots, \mathbf{x}_k)]}{n^{d(p-k+1)}} &= \lim_{n \rightarrow \infty} \int_{\mathcal{H}^k} f_x(\mathbf{x}_1) \dots f_x(\mathbf{x}_k) \frac{\Phi_{\omega}(\mathbf{x}_1, \dots, \mathbf{x}_k)}{n^{d(p+1-k)}} d\mathbf{x}_1 \dots d\mathbf{x}_k \\ &= \lim_{n \rightarrow \infty} \int_{\mathcal{H}^k} f_x(\mathbf{x}_1) \dots f_x(\mathbf{x}_k) \prod_{j=1}^d \frac{F_{\omega}(x_{1j}, \dots, x_{kj})}{n^{p+1-k}} dx_{1j} \dots dx_{kj} \end{aligned}$$

We then define $\mathbf{x}_h = [x_{h1}, \mathbf{y}_h]$ where $\mathbf{y}_h = [x_{h2}, \dots, x_{hd}]$, for $h = 1, \dots, k$ and we integrate first with respect to the variables x_{11}, \dots, x_{k1} obtaining

$$\lim_{n \rightarrow \infty} \frac{\mathbb{E}[\Phi_{\omega}(\mathbf{x}_1, \dots, \mathbf{x}_k)]}{n^{d(p-k+1)}} = \lim_{n \rightarrow \infty} \int_{[-\frac{1}{2}, \frac{1}{2}]^{(d-1)k}} G_{\omega}(\mathbf{y}_1, \dots, \mathbf{y}_k) \prod_{j=2}^d \frac{F_{\omega}(x_{1j}, \dots, x_{kj})}{n^{p-k+1}} dx_{1j} \cdots dx_{kj}$$

where

$$G_{\omega}(\mathbf{y}_1, \dots, \mathbf{y}_k) = \int_{[-\frac{1}{2}, \frac{1}{2}]^k} \frac{F_{\omega}(x_{11}, \dots, x_{k1})}{n^{p-k+1}} f_x([x_{11}, \mathbf{y}_1]) \cdots f_x([x_{k1}, \mathbf{y}_k]) dx_{11} \cdots dx_{k1} \quad (24)$$

In [11, Appendix H] it was shown that, because of the properties of $F_{\omega}(x_{11}, \dots, x_{k1})$,

$$\lim_{n \rightarrow \infty} \int_{\mathcal{B}_{\epsilon}} \frac{F_{\omega}(x_{11}, \dots, x_{k1})}{n^{p-k+1}} dx_{11} \cdots dx_{k1} = 0$$

where

$$\mathcal{B}_{\epsilon} = \{(x_{11}, \dots, x_{k1}) \mid |x_{h1} - x_{\ell 1}| > \epsilon, \text{ for some } h, \ell\}$$

for any $\epsilon > 0$. This means that the integral in (24) can be limited to the x_{11}, \dots, x_{k1} on the diagonal

where $x_{11} = \dots = x_{k1}$. Therefore

$$\begin{aligned} \lim_{n \rightarrow \infty} G_{\omega}(\mathbf{y}_1, \dots, \mathbf{y}_k) &= \lim_{n \rightarrow \infty} \int_{[-\frac{1}{2}, \frac{1}{2}]^k} \frac{F_{\omega}(x_{11}, \dots, x_{k1})}{n^{p-k+1}} f_x([x_{k1}, \mathbf{y}_1]) \cdots f_x([x_{k1}, \mathbf{y}_k]) dx_{11} \cdots dx_{k1} \\ &= \int_{[-\frac{1}{2}, \frac{1}{2}]} \prod_{h=1}^k f_x([x_{k1}, \mathbf{y}_h]) \lim_{n \rightarrow \infty} \left(\int_{[-\frac{1}{2}, \frac{1}{2}]^{k-1}} \frac{F_{\omega}(x_{11}, \dots, x_{k1})}{n^{p-k+1}} \prod_{h=1}^{k-1} dx_{h1} \right) dx_{k1} \\ &= v(\omega) \int_{[-\frac{1}{2}, \frac{1}{2}]} \prod_{h=1}^k f_x([x_{k1}, \mathbf{y}_h]) dx_{k1} \end{aligned} \quad (25)$$

Note that the limit

$$v(\omega) = \lim_{n \rightarrow \infty} \int_{[-\frac{1}{2}, \frac{1}{2}]^{k-1}} \frac{F_{\omega}(x_{11}, \dots, x_{k1})}{n^{p-k+1}} \prod_{h=1}^{k-1} dx_{h1}$$

does not depend on x_{k1} and the coefficient $v(\omega) \in [0, 1]$ is described in [9].

Next, iterating this procedure by integrating over the variables, x_{1j}, \dots, x_{kj} , $j = 2, \dots, d$ we finally get

$$\begin{aligned} \lim_{n \rightarrow \infty} \frac{\mathbb{E}[\Phi_{\omega}(\mathbf{x}_1, \dots, \mathbf{x}_k)]}{n^{d(p-k+1)}} &= v(\omega)^d \int_{[-\frac{1}{2}, \frac{1}{2}]^d} f_x(x_{k1}, \dots, x_{kd})^k dx_{k1} \cdots dx_{kd} \\ &= v(\omega)^d \int_{\mathcal{H}} f_x(\mathbf{x}_k)^k d\mathbf{x}_k \\ &= v(\omega)^d I_k \end{aligned} \quad (26)$$

where we defined $I_k = \int_{\mathcal{H}} f_x(\mathbf{x}_k)^k d\mathbf{x}_k$. It follows that

$$M_{p,d,\beta,x} = \sum_{k=1}^p \beta^{p-k} I_k \sum_{\omega \in \Omega_{p,k}} v(\omega)^d$$

which proves the theorem. Note that when the entries of $\mathbf{x}_q = [x_{q1}, \dots, x_{qd}]^T$ are independent with continuous distribution $f_{x,j}(z_j)$ such that $f_x(\mathbf{x}) = \prod_{j=1}^d f_{x,j}(x_j)$, we have $I_k = \prod_{j=1}^d I_{k,j}$ with $I_{k,j} = \int_{[-1/2, 1/2]} f_{x,j}(x)^k dx$.

APPENDIX B

PROOF OF THEOREM 5.2

From Theorem 5.1 and the definition of I_k , we have that

$$\begin{aligned} M_{p,d,\beta,x} &= \sum_{k=1}^p \beta^{p-k} I_k \sum_{\boldsymbol{\omega} \in \Omega_{p,k}} v(\boldsymbol{\omega})^d \\ &= \int_{\mathcal{H}} \sum_{k=1}^p \beta^{p-k} f_x(\mathbf{z})^k \sum_{\boldsymbol{\omega} \in \Omega_{p,k}} v(\boldsymbol{\omega})^d d\mathbf{z}. \end{aligned} \quad (27)$$

Next, we define the set \mathcal{A} where $f_x(\mathbf{z})$ is strictly positive as

$$\mathcal{A} = \{\mathbf{z} \in \mathcal{H} | f_x(\mathbf{z}) > 0\}$$

Note that for $\mathbf{z} \in \mathcal{H} \setminus \mathcal{A}$ the contribution to the integral in (27) is zero. Thus,

$$\begin{aligned} M_{p,d,\beta,x} &= \int_{\mathcal{A}} \sum_{k=1}^p \beta^{p-k} f_x(\mathbf{z})^k \sum_{\boldsymbol{\omega} \in \Omega_{p,k}} v(\boldsymbol{\omega})^d d\mathbf{z} \\ &= \int_{\mathcal{A}} f_x(\mathbf{z})^p \sum_{k=1}^p \beta^{p-k} f_x(\mathbf{z})^{k-p} \sum_{\boldsymbol{\omega} \in \Omega_{p,k}} v(\boldsymbol{\omega})^d d\mathbf{z} \\ &= \int_{\mathcal{A}} f_x(\mathbf{z})^p \sum_{k=1}^p \beta'(\mathbf{z})^{p-k} \sum_{\boldsymbol{\omega} \in \Omega_{p,k}} v(\boldsymbol{\omega})^d d\mathbf{z} \\ &= \int_{\mathcal{A}} f_x(\mathbf{z})^p M_{p,d,\beta'(\mathbf{z}),u} d\mathbf{z} \end{aligned} \quad (28)$$

where for any $\mathbf{z} \in \mathcal{A}$, $M_{p,d,\beta'(\mathbf{z})}$ is the p -th moment of $\mathbf{V}\mathbf{V}^H$ when the phases are uniformly distributed in \mathcal{H} and the ratio $\beta'(\mathbf{z})$ is given by

$$\beta'(\mathbf{z}) = \frac{\beta}{f_x(\mathbf{z})}$$

Note also that (28) holds for $p \geq 1$ since, by definition, the zero-th moment of any distribution is equal to 1. Expression (28) allows us to write the moments of $\mathbf{V}\mathbf{V}^H$ for any distribution $f_x(\mathbf{z})$, given the moments for uniformly distributed phases. Likewise, it is possible to describe the LSD of $\mathbf{V}\mathbf{V}^H$, for any continuous $f_x(\mathbf{z})$, in terms of the LSD obtained for uniformly distributed phases. Indeed, let us denote the Laplace transform of $f_{\lambda,x}(d, \beta, z)$ by $L_{\lambda,x}(d, \beta, s)$ if it exists. Then, whenever the sum converges

$$L_{\lambda,x}(d, \beta, s) = \sum_{p=0}^{\infty} \frac{s^p}{p!} M_{p,d,\beta,x}$$

Since $M_{0,d,\beta,x} = 1$ for any distribution, using (28) we obtain:

$$\begin{aligned}
L_{\lambda,x}(d, \beta, s) &= 1 + \sum_{p=1}^{\infty} \frac{s^p}{p!} \int_{\mathcal{A}} f_x(\mathbf{z})^p M_{p,d,\beta'(\mathbf{z}),u} d\mathbf{z} \\
&= 1 - |\mathcal{A}| + |\mathcal{A}| + \int_{\mathcal{A}} \sum_{p=1}^{\infty} \frac{f_x(\mathbf{z})^p s^p}{p!} M_{p,d,\beta'(\mathbf{z}),u} d\mathbf{z} \\
&= 1 - |\mathcal{A}| + \int_{\mathcal{A}} \sum_{p=0}^{\infty} \frac{f_x(\mathbf{z})^p s^p}{p!} M_{p,d,\beta'(\mathbf{z}),u} d\mathbf{z} \\
&= 1 - |\mathcal{A}| + \int_{\mathcal{A}} L_{\lambda,u}(d, \beta'(\mathbf{z}), f_x(\mathbf{z})s) d\mathbf{z}
\end{aligned} \tag{29}$$

where $|\mathcal{A}|$ is the measure of \mathcal{A} and $L_{\lambda,u}(d, \beta, s)$ is the Laplace transform of $f_{\lambda,u}(d, \beta, z)$. By using the properties of the Laplace transform and by taking its inverse, we finally get

$$f_{\lambda,x}(d, \beta, z) = (1 - |\mathcal{A}|) \delta(z) + \int_{\mathcal{A}} \frac{1}{f_x(\mathbf{z})} f_{\lambda,u} \left(d, \frac{\beta}{f_x(\mathbf{z})}, \frac{z}{f_x(\mathbf{z})} \right) d\mathbf{z}. \tag{30}$$

We can rewrite the second term of (30) by defining the cumulative density function

$$G_x(y) = \frac{1}{|\mathcal{A}|} |\{\mathbf{z} \in \mathcal{A} | f_x(\mathbf{z}) \leq y\}|$$

for $y > 0$. By using the corresponding probability density function, $g_x(y)$, and Lebesgue integration, we can rewrite (30) as in (11).

APPENDIX C

COROLLARY 5.1

From the result in (11) and from the assumption $f_x(\mathbf{z}) > 0 \forall \mathbf{z} \in \mathcal{H}$ (i.e., $|\mathcal{A}| = 1$), we have

$$f_{\lambda,x}(d, \beta, z) = \int_0^\infty \frac{g_x(y)}{y} f_{\lambda,u} \left(d, \frac{\beta}{y}, \frac{z}{y} \right) dy$$

Then, from the definition of $f_{x'}(\mathbf{z})$ given in (12) it follows that $G_{x'}(y) = G_x(cy)$ and, by consequence, $g_{x'}(y) = c g_x(cy)$. Therefore, from (13) we have:

$$\begin{aligned}
f_{\lambda,x'}(d, \beta, z) &= (1 - c) \delta(z) + c \int_0^\infty \frac{g_{x'}(y)}{y} f_{\lambda,u} \left(d, \frac{\beta}{y}, \frac{z}{y} \right) dy \\
&= (1 - c) \delta(z) + c^2 \int_0^\infty \frac{g_x(cy)}{y} f_{\lambda,u} \left(d, \frac{\beta}{y}, \frac{z}{y} \right) dy \\
&= (1 - c) \delta(z) + c^2 \int_0^\infty \frac{g_x(y)}{y} f_{\lambda,u} \left(d, \frac{c\beta}{y}, \frac{cz}{y} \right) dy \\
&= (1 - c) \delta(z) + c^2 f_{\lambda,x}(d, c\beta, cz)
\end{aligned}$$

APPENDIX D

COROLLARY 5.3

From the expression of the moments given in Theorem 5.1 and the results in [9], it is easy to show that for uniformly distributed phases, we have:

$$\lim_{\beta \rightarrow 0} M_{p,d,\beta,x} = 1$$

for any $p \geq 0$. It immediately follows that

$$\lim_{\beta \rightarrow 0} f_{\lambda,u}(d, \beta, z) = \delta(z - 1)$$

where $\delta(z)$ is the Dirac's delta function. By applying this result to (11), we get

$$\begin{aligned} \lim_{\beta \rightarrow 0} f_{\lambda,x} \left(d, \frac{\beta}{y}, \frac{z}{y} \right) &= (1 - |\mathcal{A}|) \delta(z) + |\mathcal{A}| \int_0^\infty \frac{g_x(y)}{y} \delta \left(\frac{z}{y} - 1 \right) dy \\ &= (1 - |\mathcal{A}|) \delta(z) + |\mathcal{A}| \int_0^\infty \frac{g_x(z/w)}{w} \delta(w - 1) dw \\ &= (1 - |\mathcal{A}|) \delta(z) + |\mathcal{A}| g_x(z). \end{aligned} \quad (31)$$

APPENDIX E

COROLLARY 5.2

By using the definition of the η -transform and the result in (11), we obtain:

$$\begin{aligned} \eta_x(d, \beta, \gamma) &= \mathbb{E} \left[(\gamma\lambda + 1)^{-1} \right] \\ &= \int_0^\infty \frac{1}{\gamma z + 1} f_{\lambda,x}(d, \beta, z) dz \\ &= \int_0^\infty \frac{1 - |\mathcal{A}|}{\gamma z + 1} \delta(z) + |\mathcal{A}| \int_0^\infty \frac{g_x(y)}{y} \int_0^\infty \frac{1}{\gamma z + 1} f_{\lambda,u} \left(d, \frac{\beta}{y}, \frac{z}{y} \right) dz dy \\ &= 1 - |\mathcal{A}| + |\mathcal{A}| \int_0^\infty g_x(y) \int_0^\infty \frac{1}{\gamma y z + 1} f_{\lambda,u} \left(d, \frac{\beta}{y}, z \right) dz dy \\ &= 1 - |\mathcal{A}| + |\mathcal{A}| \int_0^\infty g_x(y) \eta_u \left(d, \frac{\beta}{y}, \gamma y \right) dy. \end{aligned} \quad (32)$$

Then, by considering that $\text{MSE}_\infty = \eta_x(d, \beta, \gamma/\beta)$, the expression of the asymptotic MSE immediately follows.

APPENDIX F

COROLLARY 5.4

In Appendix 5.3 we have shown that $\lim_{\beta \rightarrow 0} f_{\lambda,u}(d, \beta, z) = \delta(z - 1)$. From the definition of the η -transform, it follows that $\lim_{\beta \rightarrow 0} \eta_u(d, \beta, \gamma) = \frac{1}{\gamma+1}$ and $\lim_{\beta \rightarrow 0} \eta_u(d, \beta, \gamma/\beta) = 0$. Thus, from (14)

we have:

$$\begin{aligned}
\lim_{\beta \rightarrow 0} \eta_x(d, \beta, \gamma) &= 1 - |\mathcal{A}| + |\mathcal{A}| \int_0^\infty g_x(y) \left(\lim_{\beta \rightarrow 0} \eta_u \left(d, \frac{\beta}{y}, \gamma y \right) \right) dy \\
&= 1 - |\mathcal{A}| + |\mathcal{A}| \int_0^\infty \frac{g_x(y)}{\gamma y + 1} dy \\
&= 1 - |\mathcal{A}| + |\mathcal{A}| \eta_g(\gamma)
\end{aligned} \tag{33}$$

where we defined $\eta_g(\gamma) = \int_0^\infty \frac{g_x(y)}{\gamma y + 1} dy$. As a consequence,

$$\begin{aligned}
\lim_{\beta \rightarrow 0} \eta_x(d, \beta, \gamma/\beta) &= 1 - |\mathcal{A}| + |\mathcal{A}| \int_0^\infty g_x(y) \left(\lim_{\beta \rightarrow 0} \eta_u \left(d, \frac{\beta}{y}, \frac{\gamma y}{\beta} \right) \right) dy \\
&= 1 - |\mathcal{A}|.
\end{aligned} \tag{34}$$

REFERENCES

- [1] D. E. Culler and H. Mulder, *Smart sensors to network the world*, Scientific American, June 2004.
- [2] M. Perillo, Z. Ignjatovic, and W. Heinzelman, “An energy conservation method for wireless sensor networks employing a blue noise spatial sampling technique,” *International Symposium on Information Processing in Sensor Networks (IPSN 2004)*, Apr. 2004.
- [3] R. Willett, A. Martin, and R. Nowak, “Backcasting: adaptive sampling for sensor networks,” *International Symposium on Information Processing in Sensor Networks (IPSN 2004)*, Apr. 2004.
- [4] F. A. Marvasti, *Nonuniform sampling: Theory and practice*, Kluwer Academic: Plenum, New York, 2001.
- [5] D. Ganesan, S. Ratnasamy, H. Wang, and D. Estrin, “Coping with irregular spatio-temporal sampling in sensor networks,” *ACM SIGCOMM*, pp. 125–130, Jan. 2004.
- [6] P. Zhao, C. Zhao, and P. G. Casazza, “Perturbation of regular sampling in shift-invariant spaces for frames,” *IEEE Transactions on Information Theory*, Vol. 52, No. 10, pp. 4643–4648, Oct. 2006.
- [7] D. S. Early and D. G. Long, “Image reconstruction and enhanced resolution imaging from irregular samples,” *IEEE Transactions on Geoscience and Remote Sensing*, Vol. 39, No. 2, pp. 291–302, Feb. 2001.
- [8] A. Nordio, C.-F. Chiasserini, and E. Viterbo, “Performance of linear field reconstruction techniques with noise and uncertain sensor locations,” *IEEE Transactions on Signal Processing*, Vol. 56, No. 8, pp. 3535–3547, Aug. 2008.
- [9] A. Nordio, C.-F. Chiasserini, and E. Viterbo, “Reconstruction of multidimensional signals from irregular noisy samples,” *IEEE Transactions on Signal Processing*, Vol. 56, No. 9, pp. 4274–4285, Sept. 2008.
- [10] A. Nordio, C.-F. Chiasserini, and E. Viterbo, “Asymptotic analysis of multidimensional jittered sampling,” *IEEE Transactions on Signal Processing*, Vol. 58, No. 1, pp. 258–268, Jan. 2010.
- [11] Ø. Ryan, and M. Debbah, “Asymptotic behavior of random Vandermonde matrices with entries on the unit circle,” *IEEE Transactions on Information Theory*, Vol. 55, No. 7, pp. 3115–3147, July 2009.
- [12] A. Tulino, and S. Verdú, *Random matrices and wireless communications*, Foundations and trends in communications and information theory, Vol. 1, No. 1, July 2004.
- [13] S. Toupis and L. Tassiulas, “Packetostatics: deployment of massively dense sensor networks as an electrostatics problem,” *IEEE Infocom*, pp. 2290–2301, 2005.
- [14] W. S. Conner, L. Krishnamurthy, and R. Want, “Making everyday life easier using dense sensor networks,” *Ubicomp 2001: Ubiquitous Computing*, pp. 49–55, 2001.
- [15] 802.15.4: IEEE Standard for Information technology-Telecommunications and information exchange between systems-Local and metropolitan area networks-Specific requirements Part 15.4: Wireless Medium Access Control (MAC) and Physical Layer (PHY) Specifications for Low-Rate Wireless Personal Area Networks (WPANs), 2009.

- [16] R. Cristescu and M. Vetterli, "On the optimal density for real-time data gathering of spatio-temporal processes in sensor networks," *International Symposium on Information Processing in Sensor Networks (IPSN '05)*, Los Angeles, CA, Apr. 2005.
- [17] Y. Sung, L. Tong, and H. V. Poor, "Sensor activation and scheduling for field detection in large sensor arrays," *International Symposium on Information Processing in Sensor Networks (IPSN '05)*, Los Angeles, CA, Apr. 2005.
- [18] M. C. Vuran, Ö. B. Akan, and I. F. Akyildiz, "Spatio-temporal correlation: theory and applications for wireless sensor networks," *Computer Networks*, Vol. 45, No. 3, pp. 245–259, June 2004.
- [19] Y. Rachlin, R. Negi, and P. Khosla, "Sensing capacity for discrete sensor network applications," *International Symposium on Information Processing in Sensor Networks (IPSN'05)*, Los Angeles, CA, Apr. 2005.
- [20] M. Dong, L. Tong, and B. M. Sadler, "Impact of data retrieval pattern on homogeneous signal field reconstruction in dense sensor networks," *IEEE Transactions on Signal Processing*, Vol. 54, No. 11, pp. 4352–4364, Nov. 2006.
- [21] P. Marziliano and M. Vetterli, "Reconstruction of irregularly sampled discrete-time bandlimited signals with unknown sampling locations," *IEEE Transactions on Signal Processing*, Vol. 48, No. 12, Dec. 2000, pp. 3462–3471.
- [22] O. Ryan, and M. Debbah, "Convolution operations arising from Vandermonde matrices," <http://www.citebase.org/abstract?id=oai:arXiv.org:0910.4624>, 2009.
- [23] G. H. Tucci and P. A. Whiting, "Eigenvalue results for large scale random Vandermonde matrices with unit complex entries," *submitted to IEEE Trans. on Information Theory*, 2010.
- [24] V. A. Marčenko and L. A. Pastur, "Distribution of eigenvalues for some sets of random matrices," *USSR Sbornik*, Vol. 1, pp. 457–483, 1967.
- [25] D. Moore, J. Leonard, D. Rus, and S. Teller, "Robust distributed network localization with noisy range measurements," *ACM Conference on Embedded Networked Sensor Systems (SenSys)*, Baltimore, MD, pp. 50–61, Nov. 2004.
- [26] K. Karenos, V. Kalogeraki, and S. V. Krishnamurthy, "Cluster-based congestion control for sensor networks," *ACM Transactions on Sensor Networks*, Vol. 4, No. 1, Jan. 2008.
- [27] J. Kim, W. Lee, E. Kim, J. Kim, C. Lee, S. Kim, and S. Kim, "On energy-aware dynamic clustering for hierarchical sensor networks," *Embedded and Ubiquitous Computing*, pp. 460–469, Nov. 2005.
- [28] C. Y. Jung, H. Y. Hwang, D. K. Sung, and G. U. Hwang, "Enhanced Markov chain model and throughput analysis of the slotted CSMA/CA for IEEE 802.15.4 under unsaturated traffic conditions," *IEEE Transactions on Vehicular Technology*, Vol. 58, No. 1, pp. 473–478, Jan. 2009.

